THE DISTRIBUTION OF RADIUM AND PLUTONIUM IN HUMAN BONE*

CONF-8410161--3

Robert A. Schlenker
Biological and Medical Research Division
Argonne National Laboratory
Argonne, Illinois 60439

CONF-8410161--3

DE85 005025

INTRODUCTION

The dosimetry of radionuclides in bone provides information essential to the interpretation of radiation effects data. The relative biological effectiveness of different radiations is expressed as a ratio of absorbed doses, and dose or dose equivalent are the intermediaries through which the risk from one radionuclide is estimated from risk data on another. Because of the wealth of information on the skeletal effects of radiation in humans accumulated in the study of radium poisoning, bone dosimetry has played an important role in radiation protection. Historically, energy deposition in the whole skeleton was the quantity first used in radiation protection calculations for internal emitters, but recently the International Commission on Radiological Protection (ICRP) shifted to bone surface tissue dose (In78). For the alpha emitters, the experimental study of dosimetry is difficult because it must be carried out on a microscopic scale, and therefore methodology is an important aspect of the work. Traditionally, the necessary data have been collected from autoradiographs, but alpha spectrometry is being developed as a tool. This paper presents aspects of current and recent work conducted in my laboratory on the distribution of radium and plutonium near the surfaces of human bone and applications

*This work was supported by the U.S. Department of Energy under Contract No. W-31-109-ENG-38.

of the data. There are sections on methods, surface deposit thickness, radium distribution near the endosteal surface, the use of alpha spectrometry in conjunction with autoradiography, radium distribution in the mastoid, and factors affecting plutonium specific activity. Much emphasis is placed on the alpha spectrometry technique because of its usefulness and its recent application to problems of local dosimetry.

METHODS

(a) Alpha Spectrometry

Because the energy loss of alpha particles in matter is well understood, it is possible to extract information on the spatial distribution of an alpha emitter within the effective sample volume* from the alpha energy spectrum, dn/dE, of a thick embedded or unembedded bone sample. By the chain rule of differential calculus, $dn/dx = (dn/dE)(dE/dx)$, where dn/dE is the number of alpha particles reaching the detector with energies between E and E + dE, dn/dx is the number which travel distances in bone between x and x + dx before escaping into the vacuum between the sample and the detector (Sc75), and dE/dx is the stopping power. The distance spectrum, dn/dx, is closely related to the spatial distribution of the alpha emitter. For plane samples measured with a sample-to-detector distance that is much greater than the largest sample dimension, dn/dx is directly proportional to the average concentration of emitter as a function of depth beneath the surface. Because the energy resolution of surface barrier detectors is so great, typically 40 to 50 keV for alphas of 3 to 9 MeV, the resolution of the distance spectrum is also high, less than 1 μm under optimum conditions (Sc75).

By the use of stripping techniques, energy spectra of radionuclide mixtures can be resolved into separate components and the relative abundances of the nuclides established. It is also possible to obtain a quantitative calibration which permits the estimation of radionuclide concentration.

---

*The effective sample volume is the surface layer of bone to a depth of one alpha particle range.

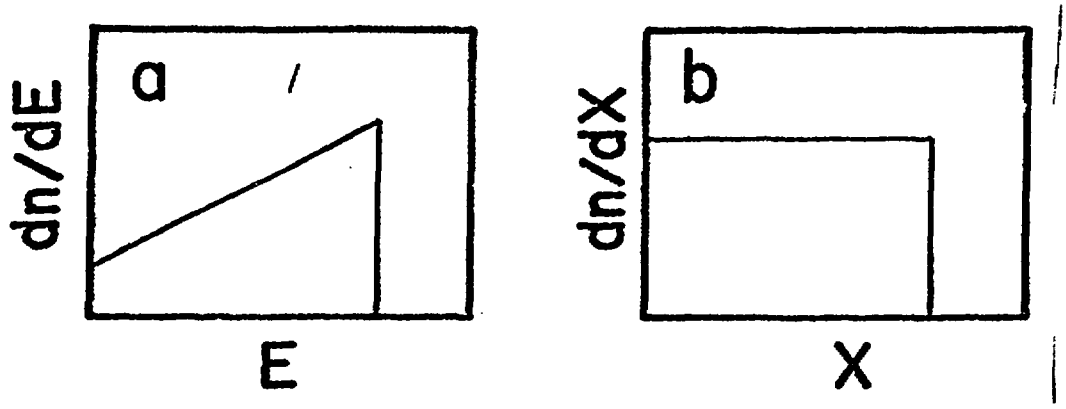

FIGURE 1 Schematic representations of (a) energy and (b) distance spectra.

Figure 1 illustrates the duality between energy and distance spectra. An energy spectrum with the shape of a linear ramp is shown to the left and beside it is the corresponding distance spectrum. In practical situations, a rectangular, i.e. constant, distance spectrum indicates a uniform spatial distribution of nuclide within the effective sample volume. It is not difficult to imagine that if the energy spectrum were concave upward, the distance spectrum would be also and if the energy spectrum were concave downward, the distance spectrum would be also. Hence, energy spectra that are concave upward, linear ramps, or concave downward strongly suggest the existence of distributions within the effective sample volume, that decrease with depth, are constant, or increase with depth, respectively.

(b) Autoradiography

For alpha detection, we use Eastman Kodak NTA emulsion plates in tight contact with 100-μm thick bone sections. Emulsion allows a faint shadow of the section (Figure 2) to be recorded on the autoradiograph as a guide to establishing registration when the autoradiograph and section are viewed simultaneously through a single set of eyepieces connected to a pair of microscopes (Mar75). The section is stained with methyl green to increase its opacity for the shadow-casting process.

For fission fragment detection, a 100-μm thick bone section laden with ^{239}Pu is placed in tight contact with a 300-μm thick sheet of Lexan plastic and the combination is exposed to thermal neutrons. Tracks are etched by floating the Lexan on 6N NaOH at temperatures

FIGURE 2 An example of shadowing on NTA emulsion. Because the photographic image is negative, the shadow is light.

between 40 and 90°C, to avoid the introduction of visible artifacts on the underside of the Lexan sheet. The bone image (Je72) assures registration between the pattern of tracks and the outline of the section.

(c) Spatial Resolution

Of the three methods, alpha spectrometry has the greatest spatial resolution. Fission track autoradiography is second. When autoradiographs are carefully developed and viewed, the position of the track entry point in Lexan relative to the bone surface can be determined with an accuracy better than 5 μm. Since the fission fragments can originate at any depth in the bone section within range of the Lexan, the actual spatial resolution is somewhat poorer than 5 μm. With alpha track autoradiography, the difficulty of achieving truly precise registration limits the resolution greatly. The shadow edge is not always easy to detect and may not correspond precisely to the outline of the section because of penumbra and non-zero section thickness. Entry points are not easy to determine, especially for short tracks that lie nearly parallel to the emulsion surface with high grain density along their full length. The best resolution achievable is probably 20-30 μm except in extremely favorable circumstances.

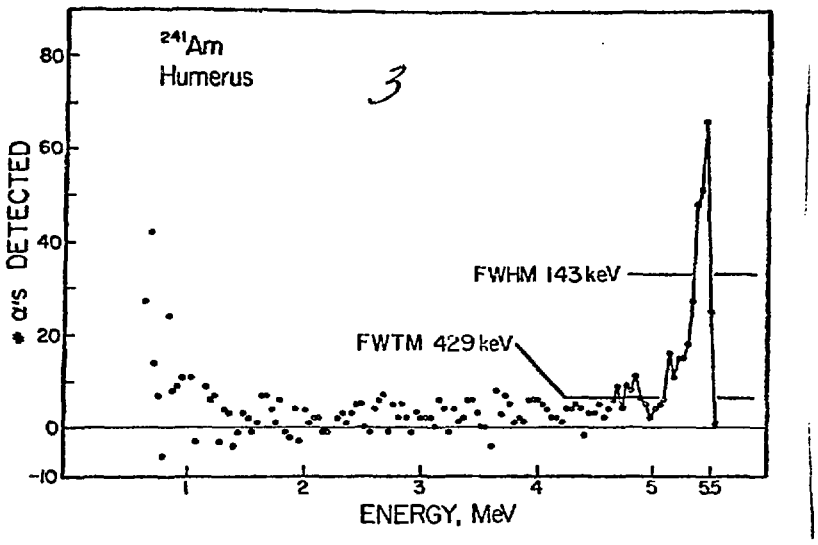

FIGURE 3 Endosteal surface alpha spectrum of ^{241}Am in human bone.

SURFACE DEPOSIT THICKNESS

Figure 3 shows the endosteal surface alpha spectrum of cortical bone from a person accidentally exposed to ^{241}Am (sample supplied by the U.S. Transuranium Registry). The spectrum peak is confined to a narrow range close to 5.49 MeV, the average energy of alpha particles emitted by disintegrating ^{241}Am. The alphas that created the peak, therefore, lost little energy and traveled only a short distance through bone before being detected and could only have originated in deposits at or near the surface. The full width at half maximum of the peak (FWHM), divided by the alpha stopping power in bone provides an index of deposit thickness, which here equals 143 keV ÷ 134 keV/μm ≈ 1.1 μm. Although the relationship between them is unknown, the index and the deposit thickness cannot differ greatly in value.

The width of the peak at its base, divided by the stopping power, provides an upper limit on deposit thickness. Non-flatness of the bone surface, small sample-detector separation, and electronic noise from the pulse amplifiers in the data collection system widen the peak and guarantee that this quotient exceeds the deposit thickness. Since the spectrum tail obscures the base of the peak, the full width at one-tenth maximum (FWTM) is used as a practical alternative to the base width. All but a negligible fraction of the peak area is included within this energy interval and the ratio of FWTM to stopping power defines a distance which is equal to, or greater than, the distance traveled by all but a negligible fraction

of the particles contributing to the peak. For Figure 3, the full width at one-tenth maximum is 429 keV and the equivalent distance is 3.2 μm.

Table 1 presents data for radionuclides deposited on the cortical endosteal surface. The data were obtained from spectra which varied widely in statistical precision. Since a more precise spectrum would be expected to yield a more precise index of deposit thickness, letters included in parentheses signify peaks in which the highest point was less than 100 counts (L), between 100 and 1000 counts (M), or in excess of 1000 counts (H). The letter B indicates a peak width that was significantly broadened by the fine structure of the alpha

Table 1. Surface deposit thickness index

Species	Nuclide	FWHM,[a] keV	Index, μm
Dog	^{212}Pb[b]	140(M)[c]	1.5
	^{224}Ra	133(H)	1.0
	^{226}Ra	178(H)	1.2
	^{228}Th	246(M,B)	1.8
Human	^{239}Pu	122(M)	0.87
	^{241}Am	143(L)	1.1

[a] Full width at half maximum.
[b] Based on the ^{212}Po daughter product.
[c] See text for explanation of letters in parentheses.

particle spectrum; for ^{228}Th, the principal emission energies are 5.42 and 5.34 MeV. Thus, the FWHM may be 0.08 MeV (80 keV) wider than if particles of a single energy were emitted in the decay of ^{228}Th. Fine structure is present with ^{239}Pu and ^{241}Am, but its effect is probably less pronounced. Because ^{212}Pb is a beta emitter, the thickness index and FWHM are based on observations of its alpha emitting daughter, ^{212}Po.

The similarity in values for the different nuclides suggests the existence of a single anatomical compartment in human and dog bone

capable of binding all radionuclides at bone surfaces regardless of their chemical properties. This compartment may be the boundary zone, represented by the lamina limitans (Mi80) in electron micrographs, between the thin layer of collagenous tissue which occurs at bone surfaces and the mineralized matrix.

RADIUM DISTRIBUTION NEAR THE ENDOSTEAL SURFACE

In the radiation protection literature, endosteal tissue dose values for bone volume seekers are calculated by assuming the radionuclide to be uniformly distributed throughout bone (In78). Advantage has been taken of the high spatial resolution of alpha spectrometry to test this assumption. In the three subjects examined so far, the radium distribution near the bone surface has been quite nonuniform, with a pronounced tendency to rise to a maximum at the surface. Figure 4 shows a spectrum from this group. Although peaks reminiscent of those found for surface seekers are prominent (compare to ^{241}Am, Figure 3), this spectrum was recorded 39 years after first exposure, at a time when radium would be classified as a volume seeker. For contrast, the spectrum of a spatially uniform source, made by grinding ashed bone to a powder and mixing it thoroughly, is shown in Figure 5 (Mau78).

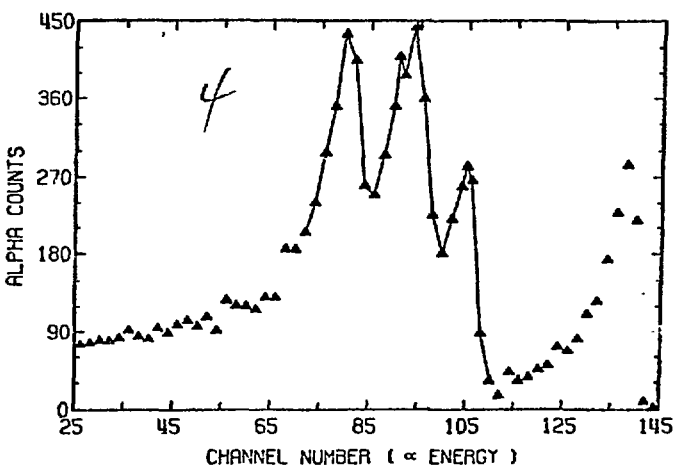

FIGURE 4 Endosteal surface alpha spectrum of ^{226}Ra and its daughters in human bone 39 years after injection (Case 01-302). From the left, the peaks correspond to ^{226}Ra, ^{210}Po, ^{222}Rn, ^{218}Po, and ^{214}Po.

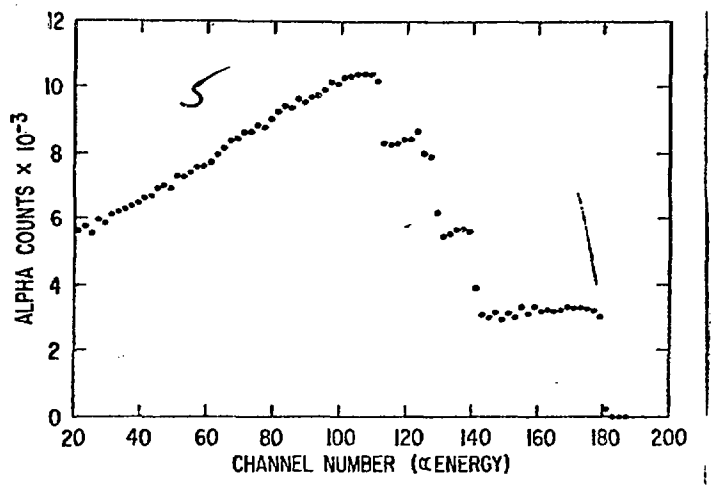

FIGURE 5 Alpha spectrum of ^{226}Ra and its daughters uniformly distributed in ashed bone. From the left, the discontinuities correspond to ^{226}Ra, ^{210}Po, ^{222}Rn, ^{218}Po, and ^{214}Po.

Radium daughter product concentrations are usually different *in vitro* than *in vivo* due to the delay between death and measurement, and to the fact that ^{222}Rn retention is affected by changes in the water content of bone. The daughter product contributions must, therefore, be separated from the total spectrum. This can be performed electronically with alpha-gamma coincidence spectrometry or mathematically by stripping away the daughter product contributions (Mau79). Figure 6 compares the results of the two methods.

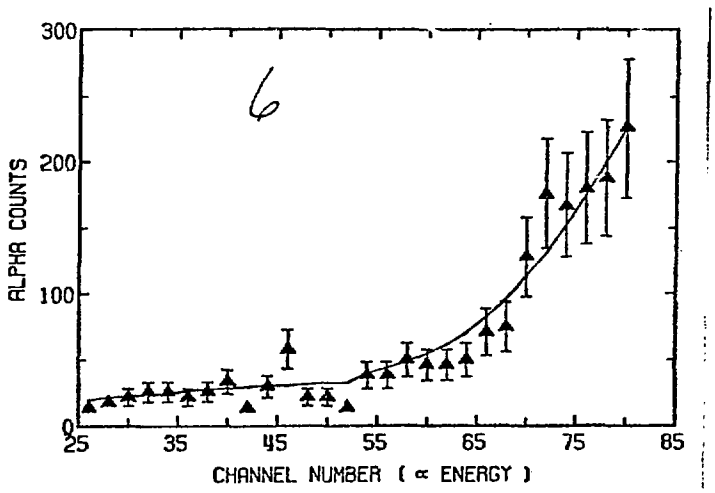

FIGURE 6 The ^{226}Ra component from Figure 4 determined by coincidence counting (points) and independently by mathematical deconvolution (solid curve).

The sample-detector geometry can be calibrated through the use of standardized solutions. A gold foil cover is molded to the sample surface. A known quantity of solution is then spread over the foil and dried and an alpha count is made to determine the fraction (g) of particle emission from the foil which is detected. For accuracy, the angular distributions of alpha particles from the foil and bone surface should be the same. This requirement is met sufficiently well when the sample-to-detector distance exceeds the detector radius and the largest sample dimension is less than the detector radius. If N_{226} is the number of ^{226}Ra alpha particles detected, N_{226}/g is the number of alphas emitted within the effective sample volume during the data collection period.

For dose-rate calculation, the endosteal tissue mass and $(dn/dx)/g$, the spatial distribution corrected for sample-detector calibration are required. The latter can be computed from the distance spectrum, an example of which is given in Figure 7 for the ^{226}Ra component of Figure 6. The former may be determined from the

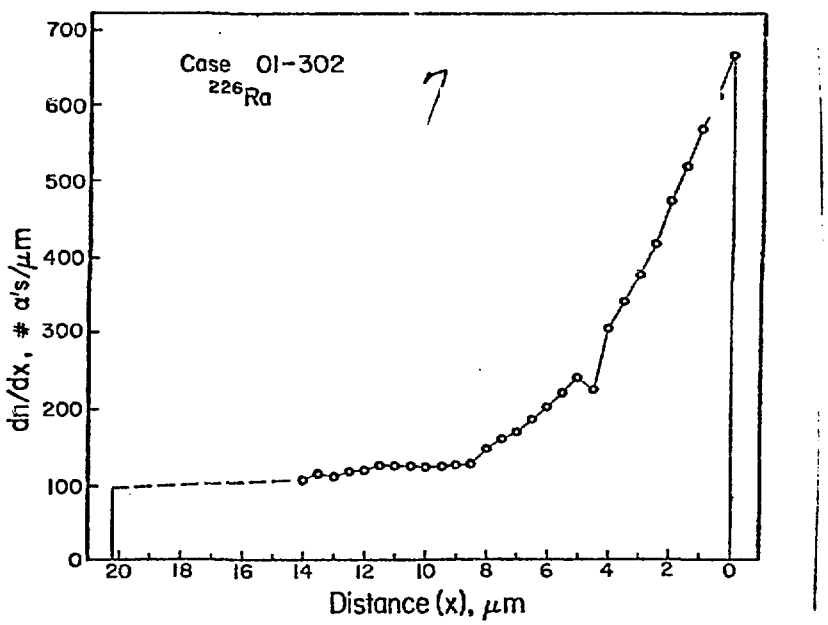

FIGURE 7 The distance spectrum for the solid curve of Figure 6. The dashed portion is an extrapolation.

sample surface area, which can be estimated from a photograph of the sample surface or calculated from the three-dimensional coordinates of the surface measured with a light section microscope. A photograph gives the sample area projected onto a plane and,

therefore, always underestimates the total area. Figure 8 shows a computer reconstruction of the sample surface from light section data. The area measured this way is 0.253 cm^2 and that measured from a photograph is 0.241 cm^2, a 5% difference.

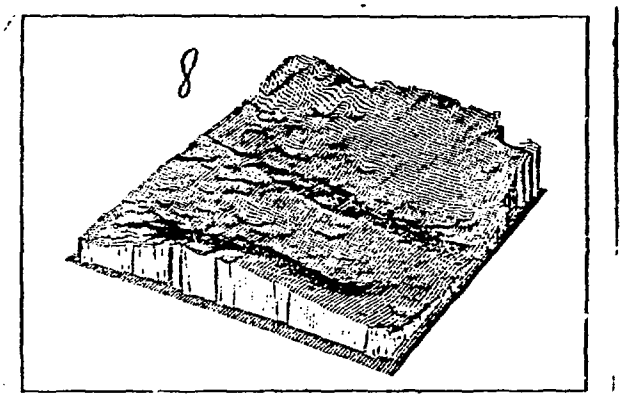

FIGURE 8 Computer reconstruction of the cortical endosteal surface of the sample used to obtain the spectrum of Figure 4.

The dose is calculated assuming a plane bone surface because the short range of the alpha particles makes the dose quite insensitive to surface irregularities. For the spatial distribution of Figure 7 and reciprocal stopping power approximated by a linear function of energy (Sc75), the dose rate, based on the calculations of Thorne (Th77), averaged over a 10-μm thick endosteal tissue layer is 0.49 rad/day, compared with 0.34 rad/day when a uniform concentration of radium is assumed.

ALPHA SPECTROMETRY IN CONJUNCTION WITH AUTORADIOGRAPHY

The analysis of track lengths and angles can be used to determine the relative abundances of different radionuclides when mixtures (Fe83,Ro56) are present in tissue sections used for autoradiography. Alpha spectrometry offers a labor-saving alternative.

The spectra from bone sections labeled with ^{226}Ra are similar to the spectrum shown in Figure 5 but often with an additional narrow ^{210}Po peak attributable to the fallout of airborne short-lived radon daughters during the storage of sections in closed containers or other environments from which radon released by the sections cannot readily escape. The long-lived beta emitter, ^{210}Pb, thus accumulates in thin deposits on the section surface and its daughter, ^{210}Po, produces a peak in alpha spectra. An example is shown in Figure 9.

The composite spectrum can be easily stripped because the nuclides within bone are uniformly concentrated as a function of depth in the effective sample volume and, therefore, all contribute linear ramp

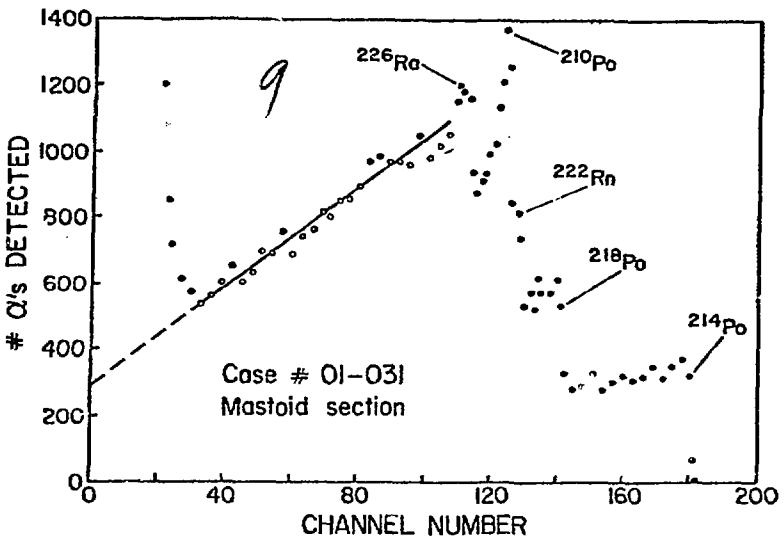

FIGURE 9 Alpha spectrum of a mastoid bone section. The straight line is used in spectrum stripping.

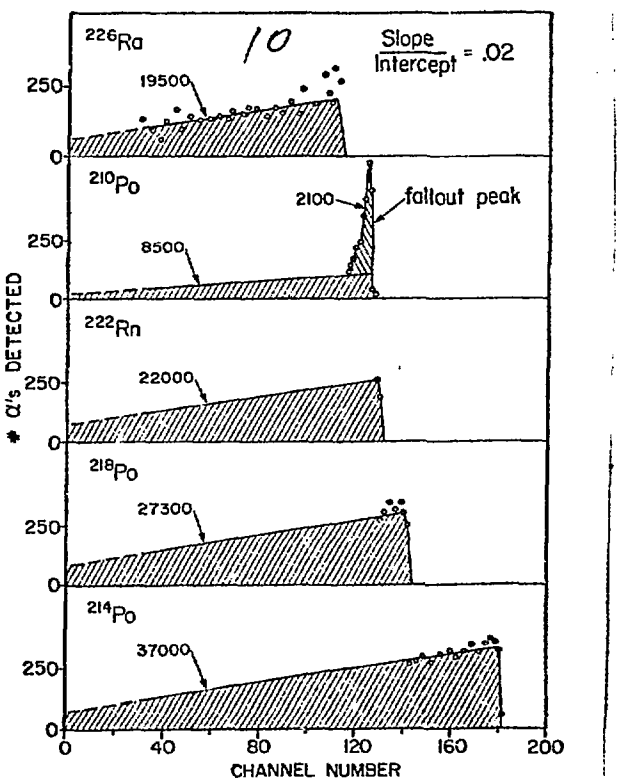

FIGURE 10 The component spectra of Figure 9, obtained by spectrum stripping as described in the text.

components with the same ratio of line slope to y-axis intercept. This ratio can be determined by fitting a straight line to the linear portion of the composite as shown in Figure 9. Linear ramps with the same ratio of slope to intercept can be fitted to the high energy ends of the components, and the components can be subtracted out one by one. The components thus obtained for Figure 9 are shown in Figure 10.

The area beneath each component (Figure 10) gives the number of alpha particles contributing to the composite spectrum, and the ratio of component area to composite area gives, with reasonable accuracy, the fraction of tracks in an autoradiograph attributable to each nuclide (Table 2).

Table 2. Percentages of alpha tracks in NTA emulsion expected to be produced by ^{226}Ra and its daughters

Nuclide	Best estimate	Ratio of areas
^{226}Ra	14	17
^{222}Rn	17	19
^{218}Po	23	23
^{214}Po	37	32
^{210}Po - total	9	9
- fallout	3	2

RADIUM DISTRIBUTION IN THE MASTOID

The mastoid, middle ear, and sinuses have been prominent sites for carcinoma induction in radium cases (Ev66). By a combination of autoradiographic measurement, bone morphometry, quantitative histology, and modeling (Ha81,Sc80,Sc83), it appears possible to determine the terminal dose rate and possibly the total lifetime dose to the epithelial tissues at risk within the mastoid and middle ear mucosa.

The epithelial cell dose is thought to be delivered by alpha particles emitted from the bone and air space (Ev66) as illustrated

for a single sinus cavity in Figure 11. The presence of radioactivity in the air space results from the production of radon gas by radium deposits in bone and the subsequent translocation of most of the radon by atomic diffusion.

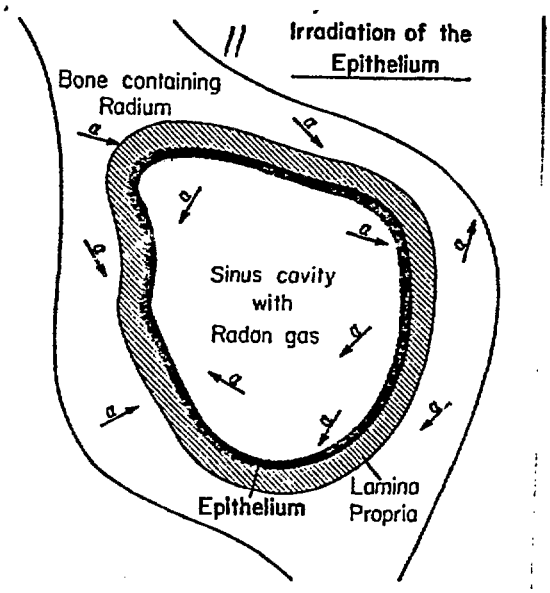

FIGURE 11 Schematic representation of a sinus showing epithelial irradiation by alpha particles from bone and from the air space.

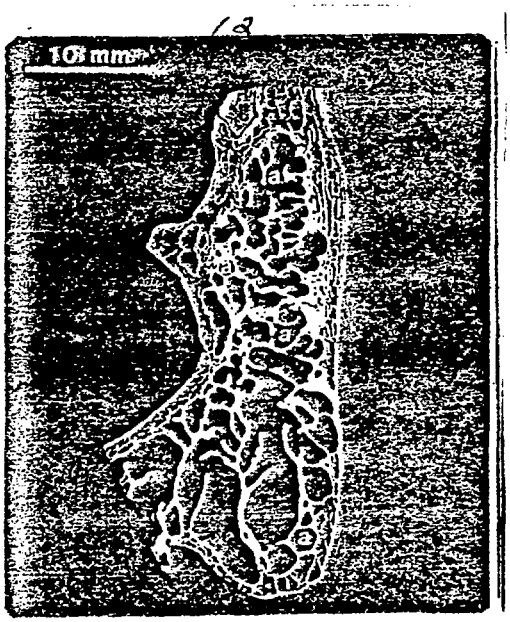

FIGURE 12 A mastoid bone section viewed by microradiography. Some air cells are identified by labels (a).

The mastoid consists of a honeycomb of air cells (Figure 12), each irradiated similarly to the sinus. There are two morphologically

distinct regions, the thin trabeculae-like bony septa that separate the air cells and the envelope of compact or cancellous bone that surrounds the air cell honeycomb. These regions differ also in their circulation. The envelope is liberally penetrated by blood vessels while the bony septa are almost totally devoid of internal circulation. Their nutrients are supplied from vessels in the mucosa.

These factors affect the fraction of radon generated within the two regions that diffuses into the air cells. Nearly all free radon will diffuse from the septa, but only half of the free radon in the envelope will diffuse toward the air cells, and much of it will be cleared by the circulation before reaching the air cells. The two regions should, therefore, be treated as distinct sources of radon and the partitioning of radium between the regions is quite important dosimetrically.

Low-resolution autoradiographs have revealed the radium distribution pattern exemplified by Figure 13, in which the radioactivity concentration appears to be lower in the septa than in the envelope. Examinations of many autoradiographs from 15 subjects showed 12 that could be classified as having low septal concentrations. This phenomenon has been examined by quantitative autoradiographic measurements at randomly selected sites within mastoid bone sections.

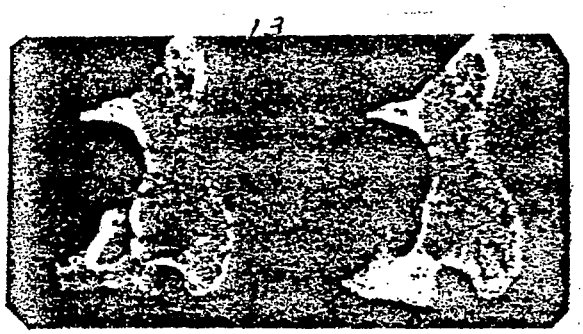

FIGURE 13 Autoradiographs of mastoid sections showing low septal and high envelope concentrations of ^{226}Ra and its daughters.

Radium specific activities estimated from track count data using an expression presented by Schlenker and Farnham (Sc76a) are given in Table 3 and verify the conclusions drawn from the visual assessment

of autoradiographs, although 14 of the 15 cases, rather than 12 of 15, show lower septal than envelope concentrations. The reason for the persistent difference between concentrations is unknown. One possibility is that blood perfusion of the envelope was much higher than of the mucosal membranes lining the septa. Another possibility is that bone formation activity was greater in the envelope, at the ages of exposure (first exposure occurred between 14 and 57 years).

Whatever the explanation, it is clear that the difference in concentrations affects the assessment of radiation dose, which, in the absence of direct observations, would be computed on the assumption that the specific activity in both regions was the same and equal to the average measured in the skeletons of these subjects. This would lead to a large error in most cases.

Table 3. ^{226}Ra specific activities in mastoid septa and envelopes measured by autoradiography and the skeletal average measured by gamma-ray detection

Case Number	^{226}Ra, pCi/g wet bone		
	Septa	Envelope	Skeletal Average
00-006	590	790	920
00-009	390	1100	720
00-027	610	840	630
01-011	320	620	2200
01-014	150	360	630
01-031	120	190	310
01-046	140	200	240
01-145	110	1400	2000
01-562	940	1800	3500
01-613	70	200	210
03-209	30	130	240
03-240	320	1200	1600
10-644	1700	1600	1700
10-831	60	150	150
10-840	80	94	130

FACTORS AFFECTING PLUTONIUM SPECIFIC ACTIVITY

Substantial differences in plutonium specific activity have been observed between different parts of the skeleton (La78) in a subject from the Langham et al. injection series (Du72) for which there are autoradiographic data (Sc76b,Sc81). Because plutonium is a surface seeker, variation in the bone surface area per gram would be expected to affect specific activity. Other important factors would be the amount of buried bone surface labeled by plutonium, and the surface concentration.

Figure 14 shows a fission track autoradiograph from the subject in question verifying the surface deposition of plutonium. The arrow points to a plutonium-labeled buried bone surface near an existing surface.

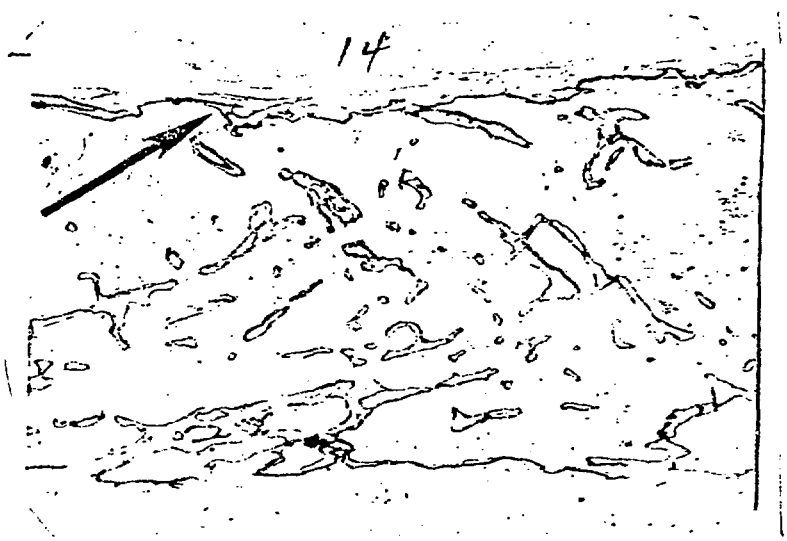

FIGURE 14 Autoradiograph of ^{239}Pu in the iliac crest. The arrow points to a plutonium laden buried bone surface.

Larsen found the plutonium specific activity in bone pieces analyzed radiochemically to be an order of magnitude higher in parts of the axial skeleton than in parts of the appendicular skeleton (La78). To determine how surface area, buried surface area and surface concentration conspire to produce such a difference, the specific activity must be expressed in terms of these quantities. The amount of plutonium on the surfaces and buried surfaces of bone is approximately $S(1 + f)C$ where S is the surface area, f times S is the area of plutonium labeled buried surface, and C is the surface

concentration. The amount of bone ash is $\rho_{ash}V$ where V is the bone volume and ρ_{ash} is the ash content per unit volume. The specific activity is, therefore, $(S/V)(1 + f)(C/\rho_{ash})$. The ratio of specific activities between two parts of the skeleton would be $[(S/V)_2/(S/V)_1][(1 + f_2)/(1 + f_1)][C_2/C_1]$.

The surface-to-volume ratio, S/V, is calculated from the perimeter to area ratio (P/A) measured from the bone section image on the autoradiograph. For cancellous bone, $S/V = (4/\pi)(P/A)$ and for compact bone, $S/V = P/A$. The ratio, f, of buried to existing surface is measured by scanning across the autoradiograph and counting the number of times a surface or a plutonium labeled buried surface is encountered. Concentration is determined by fission track counts and calibration factors.

Average values for S/V, 1 + f, and C for three anatomical regions are presented in Table 4. Specific activity ratios calculated as indicated above and those based on Larsen's radiochemical data (La78) are compared in Table 5.

Table 4. Surface-to-volume ratio, ratio of buried to existing surface, and surface plutonium concentration in Case 40-010

Region	$S/V, cm^{-1}$	1 + f	$C, pCi/cm^2$
Axial skeleton	213	1.41	1.0
Proximal femur	161	1.10	0.36
Long bone midshafts	35	1.09	0.25

Table 5. Ratios of specific activity in different regions of the skeleton, based on autoradiographic and radiochemical data

Regions	Autoradiographic	Radiochemical
Axial/femur	4.7	3.6
Axial/midshaft	31	31
Femur/midshaft	6.7	8.6

The agreement between the autoradiographic and radiochemical observations is good, verifying that S/V, f, and C are the principal determinants of specific activity in this subject.

By considering the ratios of individual factors, i.e., $(S/V)_2/(S/V)_1$, $(1 + f_2)/(1 + f_1)$ and C_2/C_1, the relative importance of each in determining the specific activity ratio can be established. These are presented in Table 6. Clearly, the difference in surface concentration is the most important determinant of the difference in specific activities between the axial skeleton and proximal femur. The difference in surface-to-volume ratios is the most important determinant of the difference in specific activities between the axial skeleton and long bone midshafts and between the proximal femur and long bone midshafts. Overall, the differences in surface-to-volume ratios and in concentrations are more important than the difference in the amount of buried bone surface.

Table 6. Ratios of the principal factors that affect the plutonium concentration in bone

Regions	$\frac{(S/V)_2}{(S/V)_1}$	$\frac{1 + f_2}{1 + f_1}$	$\frac{C_2}{C_1}$
Axial/femur	1.32	1.28	2.78
Axial/midshaft	6.09	1.29	4.00
Femur/midshaft	4.60	1.01	1.44

SUMMARY

This review of work at Argonne National Laboratory has dealt with the microdistribution of radium and plutonium in human bone with emphases on the alpha spectrometry method of measurement, the determination of deposit thickness for bone-surface seekers, the establishment of radium concentration close to the endosteal surface, the use of alpha spectrometry as a labor-saving method for determining the relative abundance of radionuclides in bone sections used for autoradiography, the measurement of radium concentration within different portions of the mastoid bone, and the explanation of why differences occur in

plutonium specific activity within different portions of the skeleton.

Some of the findings reported are that alpha spectrometry offers particularly high spatial resolution and is therefore especially well suited to the measurement of radionuclide concentrations at, and adjacent to, the endosteal surfaces. Surface deposits for isotopes of lead, radium, and the actinides are of the order of 1 μm thick. Volume deposits of ^{226}Ra can be quite nonuniform near bone surfaces and this leads to endosteal tissue dose rates that are higher than expected under the assumption of uniform volume concentration normally used for radiation protection calculations. The bony septa of the mastoid air cell system in high-dose radium cases tend to be depleted in radium relative to the envelope of the mastoid bone surrounding them, and this is expected to have a significant influence on the dosimetry of the mastoid epithelia. A combination of autoradiographic and morphometric measurements indicates that plutonium specific activities are higher in the axial than in the appendicular skeleton primarily because the axial skeleton has higher bone surface-to-volume ratios and higher bone surface concentrations of plutonium.

REFERENCES

Du72 Durbin P. W., 1972, "Plutonium in Man: A New Look at the Old Data", in Radiobiology of Plutonium (Stover B. J. and Jee W. S. S., eds.), J. W. Press, University of Utah, Salt Lake City, pp. 469-537.

Ev66 Evans R. D., "The Effect of Skeletally Deposited Alpha-Ray Emitters in Man", 1966, Brit. J. Radiol. 39, 881-895.

Fe83 Fews A. P. and Henshaw D. L., 1983, "Alpha-particle Autoradiography in CR-39: A Technique for Quantitative Assessment of Alpha Emitters in Biological Tissue", Phys. Med. Biol. 28, 459-474.

Ha81 Harris M. J. and Schlenker R. A., 1981, "Quantitative Histology of the Mucous Membrane of the Accessary Nasal Sinus and Mastoid Cavities", Ann Otol., Rhinol., Laryngol., 90, 33-37.

In78 International Commission on Radiological Protection, 1978, "Limits for Intakes of Radionuclides by Workers", ICRP Publication 30, Part 1, Pergamon Press, Oxford, 1978, p. 37.

Je72 Jee W. S. S., 1972, "^{239}Pu in Bones as Visualized by Photographic and Neutron-Induced Autoradiography", in Radiobiology of Plutonium (Stover B. J. and Jee W. S. S., eds.), J. W. Press, University of Utah, Salt Lake City, pp. 171-193.

La78 Larsen R. P., Oldham R. D., Cacic C. G., Farnham J. E. and Schneider J. R., 1978, "Distribution of Injected Plutonium in the Skeleton and Certain Soft Tissues", in Radiological and Environmental Research Division Annual Report, Center for Human Radiobiology, Argonne National Laboratory Report Number ANL-78-65, Part II, pp. 145-153.

Mar75 Marshall J. H., Groer P. G., Selman R. F., Keefe D. J. and Paul J. M., 1975, "The Microanalyzer", J. Nucl. Med. Biol. 2, 67-72. See also Radiological and Environmental Research Division Annual Report, Center for Human Radiobiology, July 1972-June 1973, Argonne National Laboratory Report Number ANL-8060, Part II, pp. 242-255.

Mau78 Mausner L. F. and Schlenker R. A., 1978, "Analysis of Thick Source Alpha Particle Spectrum from Radium and its Daughters in Bone", in Radiological and Environmental Research Division Annual Report, Center for Human Radiobiology, Argonne National Laboratory Report Number ANL-78-65, Part II, pp. 80-94.

Mau79 Mausner L. F. and Schlenker R. A., 1979, "Stripping of the Alpha Spectrum from a Bone with a Non-Uniform Depth Distribution of Radium", in Radiological and Environmental Research Division Annual Report, Center for Human Radiobiology, Argonne National Laboratory Report Number ANL-79-65, Part II, pp. 66-69.

Mi80 Miller S. C., Bowman B. M., Smith J. M. and Jee W. S. S., 1980, "Characterization of Endosteal Bone-Lining Cells from Fatty Marrow Bone Sites in Adult Beagles", Anat. Rec. 198, 163-173.

Ro56 Rotblatt J. and Ward G. B., 1956, "Analysis of the Radioactive Content of Tissues by α-Track Autoradiography", Phys. Med. Biol. 1, 57-70.

Sc75 Schlenker R. A. and Marshall J. H., 1975, "Thicknesses of the Deposits of Plutonium and Radium at Bone Surfaces in the Beagle", Health Phys. 29, 649-654.

Sc76a Schlenker R. A. and Farnham J. E., 1976, "Microscopic Distribution of ^{226}Ra in the Bones of Radium Cases: A Comparison Between Diffuse and Average ^{226}Ra Concentrations", in The Health Effects of Plutonium and Radium (Jee W. S. S., ed.), J. W. Press, University of Utah, Salt Lake City, pp. 437-449.

Sc76b Schlenker R. A., Oltman B. G. and Cummins H. T., 1976, "Microscopic Distribution of ^{239}Pu Deposited in Bone from a Human Injection Case", in The Health Effects of Plutonium and Radium (Jee W. S. S., ed.), J. W. Press, University of Utah, Salt Lake City, pp. 321-328.

Sc80 Schlenker R. A., 1980, "Dosimetry of Paranasal Sinus and Mastoid Epithelia in Radium-Exposed Humans", in Radiological and Environmental Research Division Annual Report, Center for Human Radiobiology, Argonne National Laboratory Report Number ANL-80-115, Part II, pp. 1-21.

Sc81 Schlenker R. A. and Oltman B. G., 1981, "Plutonium Microdistribution in Human Bone", in Actinides in Man and Animals (Wrenn M. E., ed.), R. D. Press, University of Utah, Salt Lake City, pp. 199-206.

Sc83 Schlenker R. A., 1983, "Mucosal Structure and Radon in Head Carcinoma Dosimetry", Health Phys. 44, 556-562.

Th77 Thorne M. C., 1977, "Aspects of the Dosimetry of Alpha-emitting Radionuclides in Bone with Particular Emphasis on ^{226}Ra and ^{239}Pu", Phys. Med. Biol. 22, 36-46.